3D simulations of an injection test done into an unsaturated porous and fractured limestone

Alain Thoraval, Y. Guglielmi, Frédéric Cappa

3D simulations of an injection test done into an unsaturated porous and fractured limestone

A. Thoraval*, Y. Guglielmi, F. Cappa
INERIS, Ecole des Mines de Nancy, FRANCE
*Corresponding author: Ecole des Mines, Parc de Saurupt, CS 14234 F-54042 Nancy cedex, alain.thoraval@ineris.fr

Abstract:

We have developed a numerical model to represent the effect of injection test in unsaturated porous and fractured rock mass. The test was conducted at the LSBB (Laboratoire Souterrain à Bas Bruit) site close to Rustrel, Vaucluse, France in the field of the French ANR project called "HPPP-CO_2".
The results underline the impact of fractures on the hydro-mechanical response of the rock-mass. Indeed fractures allow a faster dissipation of the water pressures and stress variations induced by the water injection. Back analysis lead us to also estimate the rock mass intrinsic permeability and compressibility of the injected layer.

Keywords: Nonlinear behavior, elastoplasticity, hydromechanical coupling.

1. Introduction

National and local governments show a growing concern about environmental protection on issues such as the stability of rocky slopes or the sealing of underground storage sites (hydrocarbon, radioactive and industrial waste, greenhouse gases). In all cases, hydro-mechanical couplings that occur in fractured media can affect the fluid flow and mechanical deformation processes. Both in situ measurements and model developments are needed to fully understand and predict the risks of instability and/or the fluid flow pattern into the rock mass.

The overall objective of the program HPPP_CO_2 is to develop tools and methods to characterize porous and fractured rock environments in which CO_2 could be stored. This program focuses on experiments conducted at the LSBB site close to Rustrel, Vaucluse. One contribution to this program is:

- to developed numerical model to represent the effect of injection test in unsaturated porous and fractured rock mass;
- to derive the rock-mass characteristics from numerical simulations of the in situ test done during the program.

The first step was to develop a COMSOL model including stress / strain constitutive law, two-phase flows, hydro-mechanical coupling. Some part of the model have already been validated (the part considering dry or saturated porous rock mass) through comparisons with analytical solutions [Souley et al.,2011].

The second step is about the modeling of a in situ injection test done at LSBB during the HPPP_CO_2 project.

2. Formulation of the COMSOL model

2.1 Description of the flow model

For two fluids in incompressible medium, the expressions of the flow equations are:

$$\rho_w\left(S_w\frac{\partial p_w}{\partial t}+C_{p,w}\frac{\partial p_{nw}}{\partial t}\right)+\nabla.\left(-\rho_w\frac{k_i kr_w}{\mu_w}\left(\nabla p_w+\rho_w g\nabla z\right)\right)=Q_{m,w} \quad (1)$$

$$\rho_{nw}\left(C_{p,w}\frac{\partial p_w}{\partial t}+S_{nw}\frac{\partial p_{nw}}{\partial t}\right)+\nabla.\left(-\rho_{nw}\frac{k_i kr_{nw}}{\mu_{nw}}\left(\nabla p_{nw}+\rho_{nw} g\nabla z\right)\right)=Q_{m,nw} \quad (2)$$

with:

$$S_w=-C_{p,w}+\frac{\theta_w}{K_w} \quad (3)$$

$$S_{nw}=-C_{p,w}+\frac{\theta_{nw}}{K_{nw}} \quad (4)$$

$$C_{p,w}=\frac{\partial\theta_w}{\partial p_c}=-\frac{\emptyset(1-sr_w)}{p_0}\frac{a}{(1-a)}se_w^{\frac{1}{a}}\left(1-se_w^{\frac{1}{a}}\right)^a \quad (5)$$

where:

- ρ_w and ρ_{nw} are the water and air density [kg/m^3];
- μ_w and μ_{nw} are the water and air dynamic viscosity [Pa.s];
- k_i is the intrinsic permeability of the porous medium [m^2];
- kr_w and kr_{nw} are the water and air relative permeability [m^2];
- p_w and p_{nw} are the water and air pressure [Pa];
- p_c ($= p_{nw} - p_w$) is the capillary pressure [Pa];
- sr_w the water residual saturation [-];

- se_w the water effective saturation [-];
- θ_w and θ_{nw} are the pore volumic fraction fill with water and air [-];
- $Q_{m,w}$ and $Q_{m,nw}$ are the source term for water and air [kg/m^3/s];

The capillary pressure p_c is assumed to be a function of the saturation. Van Genuchen [1980] proposes the following relation between the capillary pressure and the effective saturation of the wet fluid:

$$p_c = p_0 \, (se_w{}^{-1/a} - 1)^{(1-a)} \qquad (7)$$

Relative permeabilities can be related to saturation se_w by the empirical laws of the van Genuchten (1980) as follow:

$$kr_w = se_w{}^{b} \left(1 - \left(1 - se_w{}^{\frac{1}{a}}\right)^{a}\right)^{2} \qquad (8)$$

$$kr_{nw} = (1 - se_w)^{c} \left(1 - se_w{}^{\frac{1}{a}}\right)^{2a} \qquad (9)$$

where b and c are non dimensional characteristic parameters of the law.

2.2 Description of the hydro-mechanical model

Biot [1941] assumes that interaction between the deformability of the various constituents of a porous medium caused a readjustment of the formulation of effective stress:

$$\sigma_{eff} = \sigma_{tot} + b \, p_f \, I \qquad (10)$$

where:

- σ_{tot} is the total stress tensor (Pa),
- σ_{eff} is the effective stress tensor (Pa),
- p_f is the fluid pressure (Pa),
- I is the identity tensor,
- b is the Biot coefficient.

Considering a poro-elastic model, the effective stress tensor σ_{eff} is linked to the strain tensor ϵ:

$$\sigma_{eff} = C_0 \, \epsilon \qquad (11)$$

where C_0 is the drained elastic matrix.

From Equation (19), we got:

$$\sigma_{tot} = C_0 \, \epsilon - b \, p_f \, I \qquad (12)$$

In the Biot theory, another constitutive relation relates the increment in fluid content ζ to volumetric strain and incremental pore pressure. The fluid pore pressure is proportional to the dilation of the porous matrix and the variation of fluid content:

$$p_f = M(\, \zeta - b \, \epsilon_{vol}) \qquad (13)$$

where :

- M is the Biot modulus
- ϵ_{vol} is the trace of the strain tensor

M it is the inverse of the "constraint" storage coefficient, defined as the increase of the amount of fluid (per unit volume of rock) as a result of a unit increase of pore pressure, under constant volumetric strain:

$$\frac{1}{M} = S = \left(\frac{\partial \zeta}{\partial p_f}\right)_{\epsilon_{vol}=cte} \qquad (14)$$

In the case of an ideal porous material (characterized by a fully connected pore space and by a microscopically homogeneous and isotropic matrix material), it can be calculated from basic material properties as (see [Detournay et al., 1993] for more detail):

$$S = \frac{\emptyset}{K_f} + \frac{(b-\emptyset)}{K_s} \qquad (15)$$

where:

- $\emptyset$ is the porosity,
- K_f the fluid bulk modulus (the inverse of the fluid compressibility $\aleph_f$), and
- K_s the skeleton bulk modulus.

The Biot coefficient b can be defined in terms of the drained (K_0) and skeleton bulk (K_s) moduli:

$$b = 1 - \frac{K_0}{K_s} \qquad (16)$$

Using this expression, the storage coefficient *S* is then calculated by:

$$S = \frac{1}{M} = \frac{\emptyset}{K_f} + \frac{(b-\emptyset)(1-b)}{K_0} \qquad (17)$$

If we consider a single-phase flow in compressible medium (taking into account the hydro-mechanical coupling) the flow equation is modified as followed:

$$\rho_f \left(\frac{\emptyset}{K_f} + \frac{(b-\emptyset)(1-b)}{K_0}\right)\frac{\partial p_f}{\partial t} + \nabla\left(\rho_f \left(-\frac{k_i}{\mu_f}\left(\nabla p_f + \rho_f g \nabla z\right)\right)\right) = -\rho_f \, b \, \frac{\partial(\epsilon_{vol})}{\partial t} \qquad (18)$$

An additional equation has to be considered related to solid deformation under purely gravitational load (where inertial effects are neglected):

$$-\nabla . \sigma_{tot} = \rho_R . g = (\rho_R{}^0 + \emptyset \rho_w) g \qquad (19)$$

where:

- ρ_R is the saturated density [kg/m^3];
- $\rho_R{}^0$ is the dry density [kg/m^3].

For two-phase flow in compressible medium, the storage coefficient S_w and S_{nw} and the source term $Q_{m,w}$ and $Q_{m,nw}$ are modified in equation (1) and (2) in order to include the mechanical impact:

$$S_w = -C_{p,w} + \frac{\theta_w}{K_w} + \frac{(b-\theta_w)(1-b)}{K_0} \quad (20)$$

$$S_{nw} = -C_{p,w} + \frac{\theta_{nw}}{K_{nw}} + \frac{(b-\theta_{nw})(1-b)}{K_0} \quad (21)$$

$$Q_{m,w} = -\rho_w\, b\, \frac{\theta_w}{\phi} \frac{\partial(\epsilon_{vol})}{\partial t} \quad (22)$$

$$Q_{m,nw} = -\rho_{nw}\, b\, \frac{\theta_{nw}}{\phi} \frac{\partial(\epsilon_{vol})}{\partial t} \quad (23)$$

Equation (19) is also rewritten as follow:

$$-\nabla.\sigma_{tot} = (\rho_R{}^r).g = (\rho_R{}^0 + \theta_w \rho_w + \theta_{nw} \rho_{nw}).g \quad (24)$$

where $\rho_R{}^r$ is the real density [kg/m^3].

Some part of this model have already been validated (the part considering dry or saturated porous rock mass) through comparisons with analytical solution [Souley et al., 2011].

3. Description of the in situ experiment

An injection test has been realized in July 2010 into a 25 m long vertical borehole. Figure 1 shows a zoom where the HPPP sensor has been set about 17 m below the gallery floor.

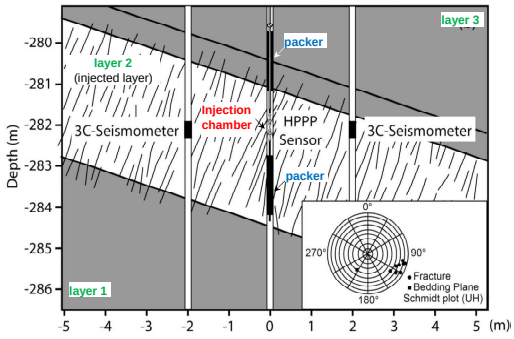

Figure 1. Detailed of the experimental injection zone and stereographic projection of the main fracture planes.

Figure 2 shows the measurements during the hydraulic injection:

- when the injection starts, the flow and pressure in the injection chamber gradually increases during the first 840 seconds, reaching maximum values of about 59 liters/min and 3.5 MPa, respectively. These values are maintained almost constant during 520 s, the period from 840 to 1360 s, then gradually decrease until it reaches 0 liter/min, from 1360 to 2050 s;
- the change in pressure is accompanied by a mechanical displacement due to the rock-mass strain and to fracture opening and shear in the vicinity of the injection. The maximum measured variation is about 20 and 30 µm for respectively the axial and shear displacements;
- no seismic activity is detected during the phase of increased fluid pressure. The cumulative seismic energy begins to increase slowly when the pressure reaches its maximum value. A significant increase in seismic energy is recorded at 1250 seconds, and then stabilizes until the end of the injection.

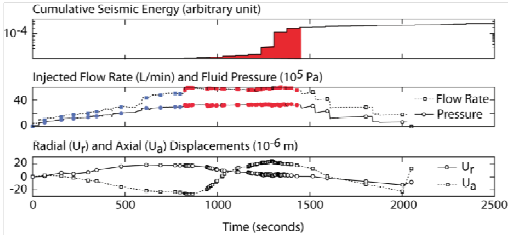

Figure 2. Experimental measurements showing: cumulative seismic energy, flow and fluid pressure, and axial and radial displacement during the hydraulic injection.

4. Set up of the 3D model

4.1 Model geometry

3D model was needed (Figure 3) to take into account the real orientation of the bedding planes and fractures. Four fractures are included into layer 2.

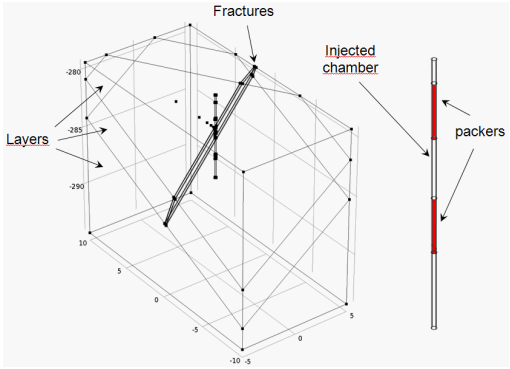

Figure 3. Model geometry.

These fractures are not taken explicitly into account. They are represented as a tabular zone. The mechanical behavior of the fractures

was represented by associating a transversely isotropic model with the layers (the plane of isotropy 1-2 corresponds to the fracture plane) considering:

$$E_3 = e\ K_n,$$

$$E_1 = 1\ K_s$$

$$G_{13} = E_1\ E_3 / (E_1 + E_3) \qquad (25)$$

where:

- K_n and K_s are the normal and shear fracture stiffnesses,
- e is the thickness of the tabular zone that represents the fracture.

The hydraulic behavior of the fractures was represented by considering for the layer an intrinsic permeability equivalent to the permeability of a fracture:

$$k_{tabular} = a_0^3/12e\ [m^2] \qquad (26)$$

where a_0 is the initial fracture hydraulic aperture.

4.2 Input data

The input data for the reference case are:

- **for the fluids:** water: density = 1000 kg/m^3 ; dynamic viscosity = 10^{-3} Pa.s ; bulk modulus = 2 10^9 Pa ; air: density = 1.28 kg/m^3 ; dynamic viscosity = 1.81 10^{-5} Pa.s ; bulk modulus = 1.41 10^5 Pa;
- **for the rock mass:** saturated density = 2650 kg/m^3; undrained Young's modulus (layer 1 & 3 / layer 2) = 25 / 10 GPa; undrained Poisson's ratio = 0.25; intrinsic permeability (layer 1 & 3 / layer 2) = 2.10^{-14} / 10^{-13} m^2 ; total porosity = 0.20 (residual porosity = 0.08) ; Biot coefficient = 0.9 ; van Genuchten parameters: a= 0.66 ; b=0.5 ; c=0.9 ; P_0=100000 Pa;
- **for the fracture:** K_n = 5 GPa/m; K_s = 0.1 GPa/m; a_0 = 2 10^{-4} => for the "equivalent" tabular zone: e = 0.04 m; E_1 = 100 MPa; E_3 = 200 MPa; G_{13} = 67 MPa; $k_{tabular}$ = 1.67 10^{-11} m^2;
- **initial conditions:** initial mechanical conditions: isotropic state of stress before gallery excavation and borehole drilling => $\sigma_v = \sigma_H = \sigma_h = \rho\ g\ h$ (with h=282 m close to the experiment location); initial hydraulical conditions: P_{air} = 0.1MPa (=1 atm); P_{water} = 0.025 MPa => water effective saturation = se_{eau} = 0.79 (considering the van Genuchten relations and parameters).

4.3 Boundary conditions

The various steps of the experiment are simulated considering the boundary conditions described into Table 1. Because of the distance from the chamber to the gallery wall, the mechanical impact of the gallery on the initial state of stress around the chamber has been neglected and we have applied a vertical stress equal to the weight of the overburden. We have also make the assumption that the packer pressure was equal the initial stress before the borehole drilling. The injected water flow is given in Figure 4.

<table>
<tr><td colspan="2">BC
(see Figure 3)</td><td>Before the borehole drilling</td><td>Borehole drilling</td><td>Packer inflating</td><td>Water injection and post injection</td></tr>
<tr><td colspan="2">t</td><td>0 – 200 s</td><td>200 – 400 s</td><td>400 – 600 s</td><td>600 – 3000 s</td></tr>
<tr><td colspan="2">(1) north face</td><td colspan="4">No displacement – No (water & air) flow</td></tr>
<tr><td colspan="2">(2) south face</td><td colspan="4">No displacement – No (water & air) flow</td></tr>
<tr><td colspan="2">(3) west face</td><td colspan="4">No displacement – No (water & air) flow</td></tr>
<tr><td colspan="2">(4) east face</td><td colspan="4">No displacement – No (water & air) flow</td></tr>
<tr><td colspan="2">(5) top face</td><td colspan="4">$\sigma = \rho g z_0$ (z_0=-279.11 m) – P_{water} = 0.025 MPa – P_{air} = 0.1 MPa</td></tr>
<tr><td colspan="2">(6) bottom face</td><td colspan="4">No displacement – No (water & air) flow</td></tr>
<tr><td rowspan="3">On borehole wall</td><td>(a) naked borehole</td><td>$\sigma_r = \rho g z$
P_{water} = 0.025 MPa
P_{air} = 0.1 MPa</td><td colspan="3">$\sigma_r = 0$ - P_{water} = 0.025 MPa – P_{air} = 0.1 MPa</td></tr>
<tr><td>(b) packers</td><td>$\sigma_r = \rho g z$
No (water & air) flow</td><td>$\sigma_r = 0$
No (water & air) flow</td><td colspan="2">$\sigma_r = \rho g z$
No (water & air) flow</td></tr>
<tr><td>(c) chamber</td><td>$\sigma_r = \rho g z$
No (water & air) flow</td><td colspan="2">$\sigma_r = 0$
No (water & air) flow</td><td>$\sigma_r = 0$
No air flow
Q_{water} = Figure 4</td></tr>
</table>

Table 1. Description of the boundary conditions

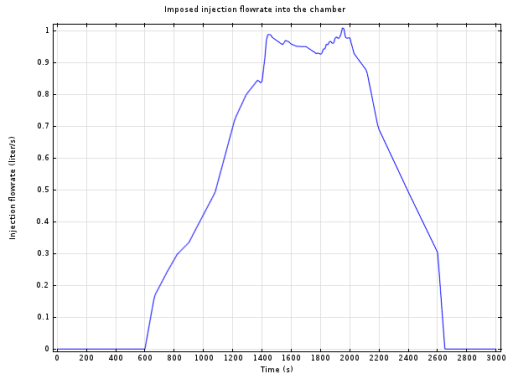

Figure 4. Hydraulical boundary condition (water flowrate) at borehole wall into the chamber to simulate the water injection test (reference case)

5. Results

5.1 Reference case

Figure 5 shows the water effective saturation evolution due to water injection in a vertical plane crossing the borehole axis. At the beginning of injection, the injected water remains roughly at the level of the chamber (between -281.15 and -282.71 m). The water begins to flow through the fractures (more permeable) to reach the bottom of layer 2. Then the saturated zone begins to expand laterally.

The water pressure variations due to injection (Figure 6) are maximal close to chamber wall into the intact rock zone. The water pressure is much smaller at the intersection of the fractures with the borehole.

5.2 Sensitivity study to back-analyse the rock mass properties

The specifications of the various runs are gathered into Table 2. Sensibility studies have been done on the value of intrinsic permeability, rock-mass cohesion and injected water flow rate.

Because of convergence problems, it was not possible (up to now) to run COMSOL up to the end of the injection phase (up to 3000 s – Figure 4). For each simulation, we have experience convergence problem at a certain injection time depending mostly on the permeability values. For case 4 (high value) this time was about 1080 s, for case 6 (low value) it was only about 70 s.

We have gathered in Table 3 sensitivity study results related to the **impact of injection on water pressure variation and water effective saturation**. We have distinguished the results into the intact rock zone and into the fracture zone. Because of permeability contrast, smaller water pressure variations are computed into the fracture zone. For the same reason, smaller water effective saturations are computed at the borehole wall (into the chamber) at the intersection with the fractures.

Comparisons between cases 1, 2 & 3 or between cases 6, 7 & 8 show that the rock-mass and fracture compressibilities have no impact on the hydraulic results.

	Young Modulus (MPa) (layer 1 & 3/ layer 2)	Intrinsic permeability (m^2) (layer 1 & 3/ layer 2)	Fracture parameters	
			K_n (GPa/m) / K_s (GPa/m) / a_0 (mm)	E_1 (GPa) / E_3 (GPa) / $k_{tabular}$ (m^2)
Reference case 1	**25 GPa / 10 GPa**	**2.10^{-14} / 10^{-13}**	**5 / 0.1 / 0.2**	**0.1 /0.2 / 1.7 10^{-11}**
Case 2	**12.5 GPa / 5 GPa**	2.10^{-14} / 10^{-13}	2.5 / 0.05 / 0.2	0.05 /0.1/ 1.7 10^{-11}
Case 3	**without mechanics**	2.10^{-14} / 10^{-13}	- / - / 0.2	- / - / 1.7 10^{-11}
Case 4	25 GPa / 10 GPa	**5.10^{-14} / 2.10^{-13}**	5 / 0.1 / 0.5	0.1 /0.2 / 2.6 10^{-10}
Case 5	25 GPa / 10 GPa	**10^{-14} / 5.10^{-14}**	5 / 0.1 / 0.2	0.1 /0.2 / 1.7 10^{-11}
Case 6	25 GPa / 10 GPa	**2.10^{-15} / 10^{-14}**	5 / 0.1 / 0.1	0.1 /0.2 / 2.1 10^{-12}
Case 7	**12.5 GPa / 5 GPa**	**2.10^{-15} / 10^{-14}**	2.5 / 0.05 / 0.1	0.05 /0.1/ 2.1 10^{-12}
Case 8	**without mechanics**	**2.10^{-15} / 10^{-14}**	- / - / 0.1	- / - / 2.1 10^{-12}

Table 2. Main input data for the various runs related to the first experiment

Otherwise, comparisons between cases 1, 4, 5 & 6 show the results are highly sensitive to the rock-mass intrinsic permeability value:

- a reduction of the rock-mass intrinsic permeability of layer 2 (from 2. 10^{-13} to 5. 10^{-14} m^2) induced an increase of the water pressure variation into the intact rock (from 0.06 to 0.214 MPa after 400 s of injection) and into the fractures (from 0.017 to 0.08 MPa after 400 s of injection). A comparison with the measurement leads us to think that the rock-mass intrinsic permeability of layer 2 must be smaller than 10^{-14} m^2;
- a reduction of the rock-mass intrinsic permeability of layer 2 (from 2. 10^{-13} to 5. 10^{-14} m^2) induced an extension of the saturated zone (from 0.45 to 0.7 m after 400 s).

	Water pressure variation at the borehole wall (MPa)		Water effective saturation	
	Intact rock zone	Fracture zone	Intact rock zone : extension of the saturated zone (m) where se_w > 0.9	Fracture zone : se_w at the borehole wall
t_{inj} (s)	200 / 400 / 600 (meas.: **1.15 / 1.75 / 2.75**)	200 / 400 / 600	200 / 400 / 600	200 / 400 / 600
Reference case 1	0.09 / 0.13 / 0.208	0.045 / 0.07 / 0.108	0.45 / 0.70 / 1.05	0.968 / 0.995 / 1
Case 2	0.09 / 0.13 / 0.207	0.045 / 0.07 / 0.108	0.45 / 0.75 / 1.1	0.968 / 0.995 / 1
Case 3	0.09 / 0.13 / 0.208	0.045 / 0.07 / 0.108	0.45 / 0.70 / 1.05	0.968 / 0.995 / 1
Case 4	0.045 / 0.06 / 0.09	0.01 / 0.017 / 0.026	0.3 / 0.45 / 0.65	0.87 / 0.896 / 0.93
Case 5	0.144 / 0.214 / -	0.053 / 0.08 / -	0.5 / 0.7 / -	0.976 / 0.998 / -
t_{inj} (s)	20 / 40 / 60 (meas.: **0.18 / 0.36 / 0.54**)	20 / 40 / 60	20 / 40 / 60	20 / 40 / 60
Case 6	0.1 / 0.21 / 0.32	0.02 / 0.05 / 0.08	0.12 / 0.22 / 0.28	0.882/ 0.967 /0.992
Case 7	0.1 / 0.21 / 0.32	0.02 / 0.05 / 0.08	0.12 / 0.22 / 0.28	0.882/ 0.967 /0.992
Case 8	0.1 / 0.21 / 0.32	0.02 / 0.05 / 0.08	0.12 / 0.22 / 0.28	0.882/ 0.967 /0.992

Table 3. Water pressure variation and water effective saturation due to water injection

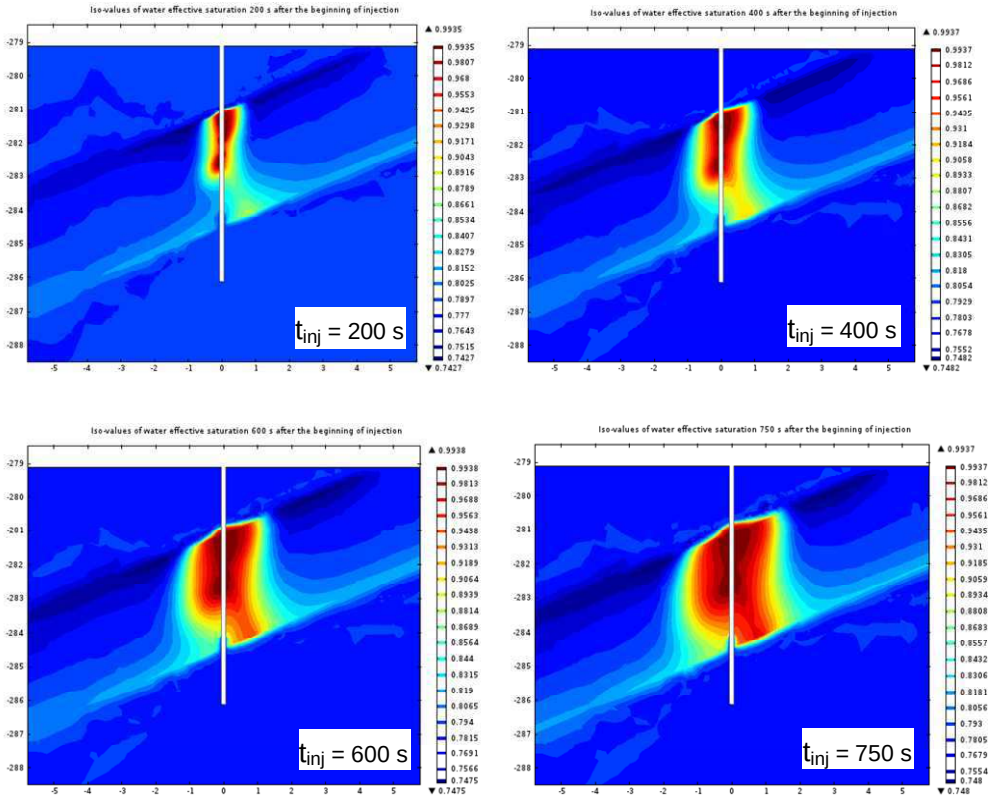

Figure 5. Iso-values of water effective saturation during water injection (for the reference case).

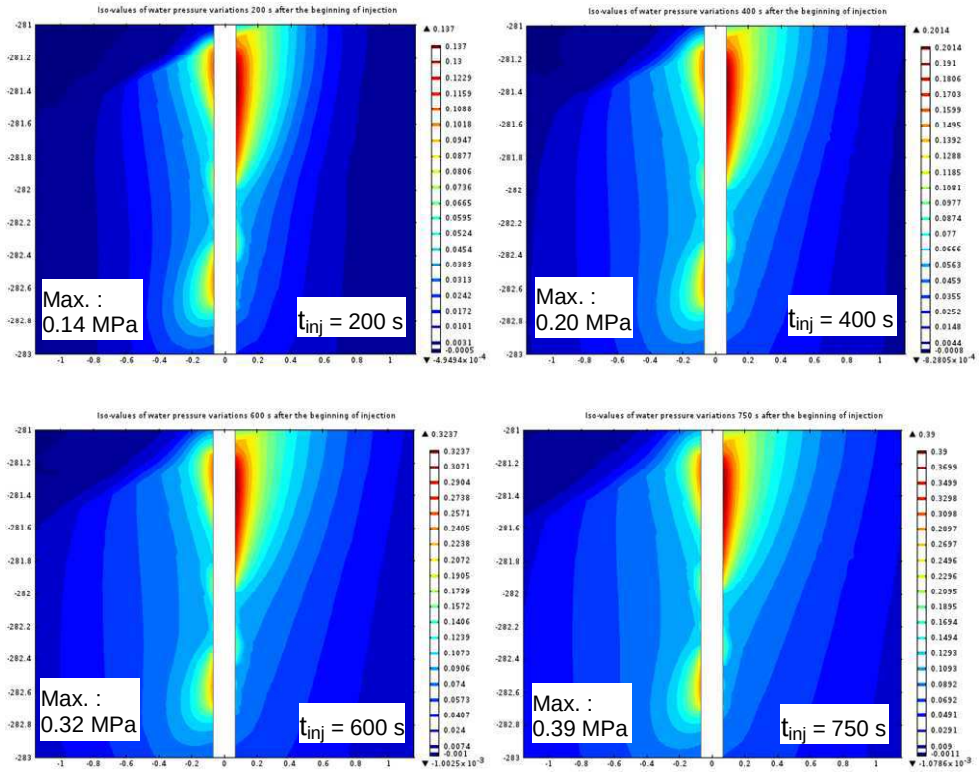

Figure 6. Iso-values of water effective saturation during water injection (for the reference case).

Table 4 gathers the main results related to **the impact of injection on displacement variations** for the sensitivity study described in Table 2. A distinction has been done between the results at the borehole wall and the results at 0.5 m inside the rock-mass to highlight the two opposite effects of pore pressure variations on displacements:

- a mechanical effect considering that the pore pressure induced by the water injection act as a confining pressure on the borehole wall,
- a hydro-mechanical coupling effect related to effective stress variations (due to the fluid pressure variations).

The importance of these two effects changes during the injection following the pressure modifications into the rock mass.

To be able to compare with the measurements done, axial displacement variations (into the direction of the borehole axis) have also been computed.

	Displacement variation (µm)		Axial displacement variation (µm)
	at the borehole wall	0.5 m from the borehole wall	
t_{inj} (s)	200 / 400 / 600	200 / 400 / 600	200 / 400 / 600 (meas.: **4.5/ 12.5 /16**)
Reference case	1.2 / -1 / -3	2.8 / 4 / 5.5	1.5 / 4.5 / 9.5
Case 2	0.5 / -8 / -12.5	5 / 8 / 10.5	4 / 12.5 / 30
Case 3	Computation without mechanics		
Case 4	0.3 / 0.5 / -1	1 / 1.5 / 2.2	0.3 / 0.7 / 1.8
Case 5	-1 / -2.5 / -	3.2 / 4.9 / -	3.5 / 7.3 / -
t_{inj} (s)	20 / 40 / 60	20 / 40 / 60	20 / 40 / 60 (meas.: **0.3 / 0.58 / 0.84**)
Case 6	0.2 / 0.1 / -2	0.3 / 1 / 2	-0.1 / -0.1 / -0.3
Case 7	0.3 / -1 / -5.5	0.6 / 2 / 4	-0.07 / 0.27 / 0.86
Case 8	Computation without mechanics		

Table 4. Water pressure variation and water effective saturation due to water injection

Comparisons between cases 1 & 2 or between cases 6 & 7) show that a reduction of the Young's modulus of layer 2 (from 10 to 5 GPa) induced an increase of the displacement variations. Comparing cases 6 to case 7 (at 60 s), these variations are increasing from -2 to -5.5 µm at borehole wall, from 2 to 4 µm at 0.5 m inside the rock-mass, from -0.3 to 0.86 µm for the axial displacements. A comparison with the measurement show that, for an intrinsic permeability choice of 10^{-14} m^2 for layer 2, the best choice for rock-mass compressibility seem close to case 7.

Considering the displacement variations with intrinsic permeability, the Young's Modulus for layer 2 must be a little bit higher than 5 GPa. Indeed, comparisons between cases 1, 4, 5 & 6 show that a reduction of the rock-mass intrinsic permeability of layer 2 (here from 2. 10^{-13} to 5. 10^{-14} m^2) induced (via the water pressure increase) an increase of the displacement variations. At 400 s, these variations are increasing: from 0.5 to -2.5 µm at borehole wall, from 1.5 to 4.9 µm at 0.5 m inside the rock-mass, from 0.7 to 7.3 µm for the axial displacements.

6. Concluding remarks

A specific COMSOL model has been developed to represent the hydro-mechanical behavior of a porous and fractured rock mass in unsaturated condition. This model has been used to simulate an in situ injection test done at LSBB site in the field of the French ANR project HPPP-CO_2.

Despite some convergence problems (for low permeability cases), the result given by the 3D model allow us:

- to underline the impact of fractures on the hydro-mechanical response of the rock-mass to water injection that leads to pressure decrease and displacement increase;
- to estimate the rock mass intrinsic permeability and compressibility of the injected layer. From the simulation done and a comparison to the measurements, we can assume: a rock-mass intrinsic permeability close to 10^{-14} m^2 and a Young's Modulus close to 5 GPa.

7. Acknowledgments

This work has been funded by the ANR "Captage de CO_2" through the "HPPP-CO_2" project.

8. References

Biot M.A., *General theory of three-dimensional consolidation*, J Appl Phys, **12**, 155–64, (1941)

Souley M., Thoraval A., *Nonlinear mechanical and poromechanical analyses: comparison with analytical solutions*, COMSOL conference, Stuttgart, oct 26-28 (2011).